CONF-9006172--1

MULTIPLE-FREQUENCY SURFACE ACOUSTIC WAVE DEVICES AS SENSORS

Antonio J. Ricco and Stephen J. Martin

Microsensor Division 1163
Sandia National Laboratories
Albuquerque, New Mexico 87185 USA

SAND--90-0139C

DE90 009972

ABSTRACT

We have designed, fabricated, and tested a multiple-frequency acoustic wave (MUFAW) device on ST-cut quartz with nominal SAW (surface acoustic wave) center frequencies of 16, 40, 100, and 250 MHz. The four frequencies are obtained by patterning four sets of input and output interdigital transducers of differing periodicities on a single substrate. Such a device allows the frequency dependence of AW sensor perturbations to be examined, aiding in the elucidation of the operative interaction mechanism(s). Initial measurements of the SAW response to the vacuum deposition of a thin nickel film show the expected frequency dependence of mass sensitivity in addition to the expected frequency independence of the magnitude of the acoustoelectric effect. By measuring changes in both wave velocity and attenuation at multiple frequencies, extrinsic perturbations such as temperature and pressure changes are readily differentiated from one another and from changes in surface mass.

INTRODUCTION

As the utility of AW (acoustic wave) devices for chemical sensing and materials characterization is explored in more detail by an increasing number of workers, it has become apparent that monitoring only the frequency change resulting from a sensor perturbation can yield less than all the available information. For example, we recently pointed out the additional insight provided by simultaneously recording changes in both acoustic wave velocity (v) and attenuation (α) when monitoring photopolymerization, acoustoelectric coupling, or liquid viscosity (1,2).

In general, the various perturbations that can affect AW propagation characteristics depend differently upon frequency (f). Furthermore, for a given perturbation, the frequency dependence of the fractional change in wave velocity, $\Delta v/v_0$, often differs in its frequency dependence from the change in wave attenuation. Thus, to further supplement the information available from acoustic wave sensors, we designed and fabricated the multifrequency acoustic wave device shown schematically in Figure 1. This MUFAW device enables the frequency dependence of perturbations to wave velocity and attenuation to be recorded. Application of such devices to problems in chemical sensing and materials characterization should make it possible to unambiguously separate from one another some of the many and varied perturbations which affect acoustic wave propagation.

In this paper, we report the design details and preliminary results from the MUFAW device. We have utilized the vacuum evaporation of a thin nickel film as a means to confirm the frequency dependence of mass sensitivity. In addition, the Ni film deposition provides an opportunity to examine a perturbation which should have no dependence on frequency, namely acoustoelectric coupling (3). Measurements of temperature and pressure effects at multiple frequencies are reported as well.

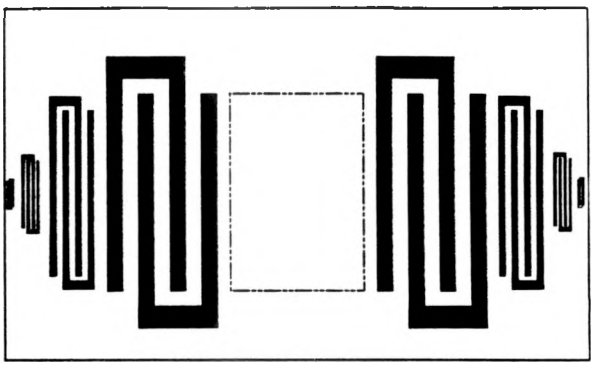

Figure 1. Schematic diagram of multifrequency acoustic wave device. Actual input and output transducers consist of 25 pairs of interdigitated electrodes for the 16 and 40 MHz transducers and 50 pairs for 100 and 250 MHz transducers. The interaction region is defined by the dashed box.

Background: Acoustoelectric Coupling

The coupling of an acoustic wave propagating in a piezoelectric substrate to charge carriers in an adjacent medium provides a novel mechanism for the study of changes in electrical conductivity in thin solid films and in solution (3,4). This acoustoelectric effect can be utilized to construct new chemical sensors and to study conductivity effects in general. For a SAW device, a surface film having sheet conductivity σ_s perturbs the wave velocity by an amount $\Delta v/v_0$ and changes the attenuation (normalized by the wavenumber, k) by an amount $\Delta\alpha/k$, according to (3):

$$\frac{\Delta v}{v_0} = -\frac{K^2}{2}\,\frac{\sigma_s^2}{\sigma_s^2 + v_0^2 C_s^2} \qquad [1]$$

$$\frac{\Delta \alpha}{k} = \frac{K^2}{2}\,\frac{v_0 C_s \sigma_s}{\sigma_s^2 + v_0^2 C_s^2}, \qquad [2]$$

where K^2 is the electromechanical coupling coefficient and C_s is the capacitance/length of the substrate ($C_s = \epsilon_0 + \epsilon_1$, the sum of the permittivities of the substrate and the region above it).

EXPERIMENTAL METHODS

Multiple-frequency acoustic wave devices were designed and fabricated in the Microsensor Division at Sandia National Laboratories. Each device has interdigital transducers of four different periodicities to excite and detect Rayleigh waves (SAWs) on ST-cut quartz at 16, 40, 100, and 250 MHz. The same transducers can excite shear-horizontal acoustic plate modes (SH-APMs) on ST-quartz at roughly 1.6 times the SAW frequencies, i.e. 25.6, 64, 160, and 400 MHz. The transducer periodicity defines the acoustic wavelength, Λ_0, at the center frequency; the width of the fingers and spaces comprising each transducer is ¼ of its periodicity. Table I lists relevant design parameters for each of the four transducers.

Devices were fabricated on 0.5 mm-thick ST-cut quartz wafers. Transducers were defined photolithographically, using an etching process, from 100 to 200 nm-thick Au-on-Cr metallization. Wafers were diamond sawed into 3.6 x 1.3 cm devices, each of which was then attached to a custom-fabricated

---

TABLE I

Design Parameters for Multifrequency Acoustic Wave Device

SAW Center Frequency, MHz	16	40	100	250
Acoustic Wavelength, μm	200	80	32	12.8
No. of Finger Pairs	25	25	50	50
Acoustic beam width,[1] $N_{A_o,1}$	50	100	100	100
Acoustic path length,[1] $N_{A_o,2}$	75	280	850	2400

[1] $N_{A_o,1}$ = length of transducer fingers in acoustic wavelengths; $N_{A_o,2}$ = center-to-center spacing between input and output transducers in acoustic wavelengths.

alumina PC board having a number of 50 Ω, lithographically defined coplanar-waveguides running from the device to contact areas along the board's periphery. 25 μm Au wire bonds were made between the transducer bonding pads and the waveguides. In some cases, several input transducers (of differing periodicity) were bonded in parallel to a single guide; corresponding output transducers were then similarly connected in parallel. PC board-mounted devices were installed in a custom-fabricated brass test case utilizing Au-plated Cu/Be spring contacts to connect the board's contact pads to SMA jacks, which were connected by coaxial cable to the external circuitry.

The electronic measurement circuitry can be configured in a number of different ways. The familiar oscillator loop can be constructed in the manner described elsewhere (5) for each input/output transducer pair. To measure oscillation frequency and device insertion loss, directionally coupled outputs from each loop are connected to a frequency counter and power meter (or vector voltmeter) *via* a computer-controlled rf multiplexer (described below), economizing on instrumentation.

The majority of the measurements reported below were made using the computer-controlled phase-locked loop configuration shown schematically in Figure 2. A 10 dB directional coupler directs a fraction of the power from a synthesized source (HP 8656B) to the reference channel of the vector voltmeter (HP 8508A). The balance of the power enters one of the MUFAW input transducers *via* the VHF multiplex card of an HP 3488A Switching & Control Unit. The M_i denote impedance matching networks (these have not yet been incorporated). The output from the device is directed to the second channel of the vector voltmeter by a second multiplexer card.

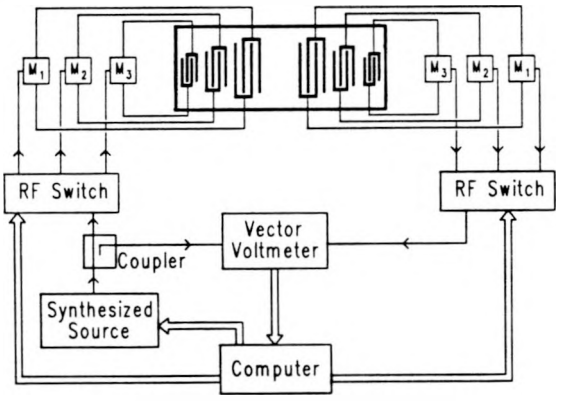

Figure 2. Schematic representation of computer-controlled phase-locked loop used to simultaneously monitor acoustic wave velocity and attenuation. Vector voltmeter records phase shift and differential power level; as sensor is perturbed, computer adjusts source frequency to keep the phase shift constant for a given transducer pair. Computer-controlled rf multiplexers (denoted "RF Switch") allow several different transducer sets having different characteristic frequencies to be probed in rapid succession. The M_i denote impedance-matching networks.

A Hewlett-Packard 9816 computer acquires differential phase and insertion loss data from the vector voltmeter in addition to setting the multiplexers to the appropriate channel and the source to the appropriate frequency. During each cycle (approximately every 3 s), the computer adjusts the source frequency sent to each input transducer in order to maintain the phase shift at a constant value. Thus, as wave velocity changes due to external perturbations, the source frequency tracks it according to:

$$\frac{\Delta f}{f_o} = \kappa \frac{\Delta v}{v_o}, \qquad [3]$$

where κ is the fraction of the acoustic path length being perturbed. Insertion loss and source frequency, along with any other varying parameter (film thickness, temperature, etc.), are then recorded as a function of time by the computer.

Thermal deposition of Ni was carried out in a cryogenically pumped vacuum system with a base pressure near 10^{-7} Torr. Radio-frequency feedthroughs allow the various acoustic wave propagation parameters to be monitored *in situ* during the process of film deposition. Metal film thicknesses are measured using a commercial (Inficon) quartz crystal microbalance (QCM).

RESULTS AND DISCUSSION

Frequency Response

Frequency response data for the MUFAW device, Figure 3, reveal Rayleigh peaks (R) at approximately 15.5, 39.3, and 97.3 MHz. Various acoustic plate modes are apparent as well. This set

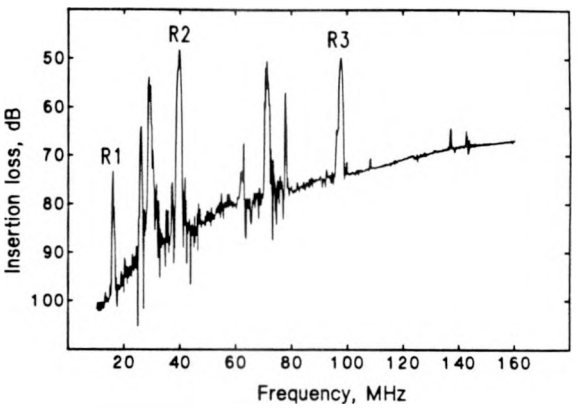

*Figure 3. Frequency response of the multifrequency acoustic wave device. Impedance matching networks have not yet been incorporated, accounting for the relatively large insertion loss of the acoustic peaks. Rayleigh peaks at 15.5, 39.3, and 97.3 MHz are indicated **R1**, **R2**, and **R3**, respectively. A number of acoustic plate modes are visible as well, including shear-horizontal acoustic plate modes at 1.6 times the frequency of **R1** and **R2**.*

of data was obtained with the transducers for these three frequencies connected in parallel. Shear-horizontal acoustic plate modes are visible near 25 and 63 MHz. The SH-APM associated with the 97 MHz SAW would normally appear near 158 MHz (6); this mode is either entirely absent or may be represented by one of the highly attenuated features near 140 MHz. This is expected: the SH-APM has displacement components on both faces of the quartz plate and, in this particular case, the back side of the plate is unpolished and is secured using adhesive to a PC board, conditions which should attenuate the wave. It is also reasonable that the two lower frequency SH-APMs are less affected by the attachment and surface finish of the quartz plate, since the propagation paths at these frequencies contain many fewer acoustic wavelengths (75 and 280 Λ_o for the 25 and 63 MHz SH-APMs, respectively, vs. 850 for the 158 MHz APM). The acoustic propagation loss, L (in dB), is proportional to the number of wavelengths in the wave path:

$$\Delta L = 54.6 n_{\Lambda_o} \frac{\Delta \alpha}{k}, \qquad [4]$$

where $n_{\Lambda_o} = \kappa N_{A_o,2}$. Furthermore, attenuation due to coupling to a viscous medium (the adhesive in this case) often increases with frequency (6,7), further obliterating the 158 MHz mode.

Not shown in Figure 3 is the region near 250 MHz. This is because there is nothing to see. For one of several devices, a feature in the vicinity of 250 MHz which might be attributed to the highest frequency SAW was recorded. In general, however, we

believe that the acoustic path between the 250 MHz transducers is so long (2400 λ_0) that diffraction of the acoustic beam (8) results in significant signal loss. In addition, any acoustic loss due to attenuation will be largest at this frequency due to the large number of wavelengths between transducers. Finally, scattering off the other transducers has the greatest effect at this frequency, both because the wave must traverse more of the other transducers and because the thickness of the metallization is a larger fraction of the acoustic wavelength.

These considerations could lead one to question our sanity in choosing this design. The advantages of the sort of design represented by Figure 1 are that a single interaction region (the dashed box) or some part thereof is probed by all the waves of various frequencies. Reversing the order of the transducers would alleviate a number of the problems mentioned above, but creates others. In a "reversed" design, a portion of the wavefronts from the low frequency transducers would pass through the various high frequency transducers, causing parts of the wavefront to arrive at the relevant output transducer out of phase, i.e. the waves would not be straight-crested. We are therefore currently considering designs which give each pair of transducers an independent path having no intervening transducers. Although this puts more stringent requirements on the point-to-point uniformity of a thin film used for chemical detection or film characterization (different regions of the film will be probed at different frequencies), it may be the best way to make the higher frequency measurements.

Nickel Deposition

Acoustoelectric coupling. The effects on SAW propagation characteristics of acoustoelectric coupling, as outlined by Eqs. 1 and 2, are revealed by the results of the experiment depicted in Figure 4, which is a plot of $\Delta v/v_0$ and $\Delta\alpha/k$ as a function of the

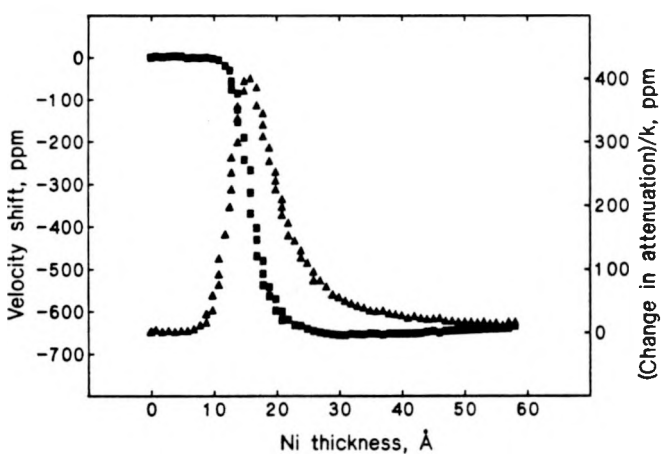

Figure 4. Experimental data showing the acoustoelectric effect in the form of fractional velocity shift (■) and normalized attenuation change (▲), both in parts per million, as a function of vacuum-evaporated nickel film thickness. Data are for a 97 MHz ST-cut quartz SAW device. The $\Delta v/v_0$ data have been corrected for the effect of mass loading.

thickness of a Ni film vacuum-evaporated onto the bare surface of a 97 MHz (single frequency) SAW device (2). It should be noted that the fractional velocity shift data of Figure 4 have been corrected for the effect of mass loading utilizing the relation (3):

$$\frac{\Delta v}{v_0} = -c_m f_0 \rho_s, \qquad [5]$$

in which c_m is the SAW mass sensitivity coefficient and ρ_s is the mass/area added to the surface. The Ni thickness recorded by the QCM was used to compute the mass/area, and this linear perturbation was subtracted from the data according to Eq. 5. The attenuation data were calculated directly from changes in the measured insertion loss using Eq. 4.

Figure 5 shows the results of the vacuum deposition of a Ni film onto the area between the transducers (as defined by the dashed box of Figure 1) of the MUFAW device. The two curves shown were obtained at 39.3 (■) and 97.3 MHz (▲) using the computer-controlled phase-locked loop configuration of Figure 2.

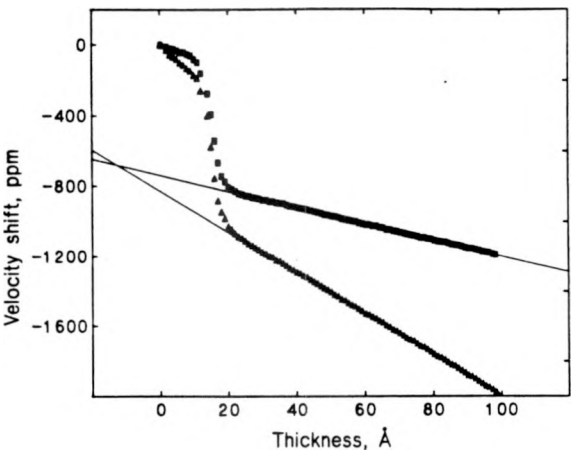

Figure 5. Effect of the evaporation of a thin Ni film on the acoustic wave velocity for the device represented by Figure 1. Data are for 39 (■) and 97 (▲) MHz SAWs. The acoustoelectric effect (represented by the sigmoidal portion of the curves) is frequency-independent in magnitude, while the ratio of the slopes in the linear, mass-loading regions of the data is 2.5, precisely the ratio of the frequencies. Straight lines are linear least-squares fits to the data between 30 and 100 Å of Ni.

Fractional velocity shift was calculated from the measured frequency change according to Eq. 3, with $\kappa = 0.25$ and 0.19 for the 39 and 97 MHz SAWs, respectively.

Eqs. 1 and 2 indicate that the magnitude of the acoustoelectric effect should be independent of frequency. Figure 5 indeed reveals that the acoustoelectric effect, which is manifested in the sigmoidal portion of the curves near 15 Å Ni thickness, is about the same for the two frequencies monitored. Measurements of propagation loss, carried out concurrently with the velocity measurements shown in Figure 5, give peak values of 190 and 220 ppm for $\Delta\alpha/k$ at 39 and 97 MHz, respectively. The difference in these values is insignificant within our estimates of their uncertainty.

Mass sensitivity. The linear regions in the data of Figure 5 are the result of mass loading. Linear least-squares fits to the data in the 30 - 100 Å thickness range, shown by the solid lines, give a measure of the coefficient of mass sensitivity. The results of these fits are slopes of -4.58 and -11.6 ppm/Å, consistent with the ratio of SAW frequencies being 2.5. The slopes yield values for c_m in Eq. 4 of 1.32 and 1.34 cm²/g-MHz for the 39 and 97 MHz SAWs, respectively. The c_m value for the 97 MHz SAW is in excellent agreement with the previously reported value of 1.34 cm²/g-MHz (9);the sensitivities at the two frequencies also agree quite well.

The oft-quoted f^2 dependence of mass sensitivity for SAW devices is based on reporting Δf alone, incorporating both the f_0 from the denominator of $\Delta f/f_0$ and the factor of f_0 shown explicitly

in Eq. 5 into the value of c_m. In fact, our measurements at multiple frequencies reveal that, for the particular test arrangement used, the short-term noise levels (in Hz) are quite comparable at 16, 39, and 97 MHz. Thus, the short-term noise-limited mass sensitivity for the 97 MHz SAW is indeed about 6.25 times greater than that of the 39 MHz SAW. (We choose to express our results in terms of $\Delta f/f_0$ due to the ease of comparison with the various models for perturbations to the wave velocity.)

Consistent and reproducible mass sensitivity results were not obtained for the 16 MHz SAW. In fact, the mass sensitivity of this mode, measured in the same manner as described above, was inconsistent from one measurement to the next, sometimes nonlinear, and in some cases exceeded that of the 39 MHz SAW. We attribute this to the fact that the acoustic wavelength at 16 MHz is a significant fraction (about 40%) of the thickness of the quartz substrate: when the thickness of the medium along which the SAW propagates becomes comparable to the acoustic wavelength, the SAW degenerates into a Lamb wave (9,10) (a type of acoustic plate mode). We are currently investigating the effect of quartz substrate thickness on this phenomenon.

Temperature & Pressure Effects

A further demonstration of the utility of multiple frequencies is provided by Figure 6. The effects of changes in temperature and pressure are displayed by plotting $\Delta\alpha/k$ *vs.* $\Delta v/v_0$. Room temperature at 1 atm pressure is taken as the arbitrary reference point at which $\Delta v/v_0 = 0$ and $\Delta\alpha/k = 0$. Each set of points surrounded by a solid boundary represents a single temperature/pressure combination. Closed symbols represent temperature changes, while open symbols are used for pressure change. The three smooth curves are approximate isobars (temperature response at constant pressure) at one atmosphere for the three frequencies examined.

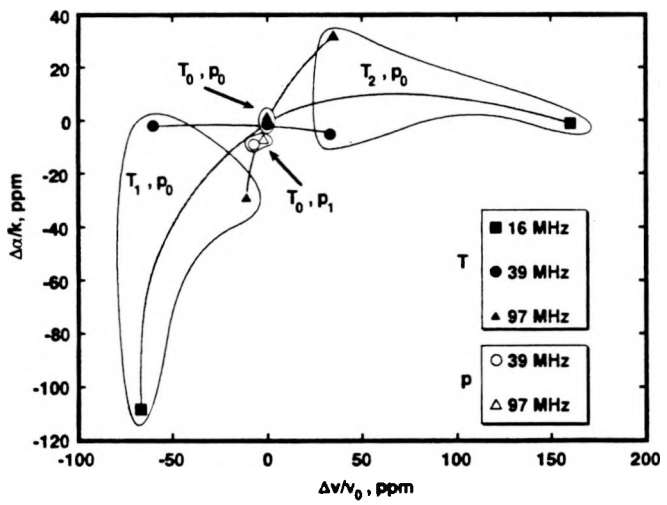

Figure 6. Change in normalized attenuation plotted against fractional velocity shift at 16 (■), 39 (●), and 97 (▲) MHz for the device of Figure 1; temperature and pressure are the variable parameters. T_0 = 24 C and p_0 = 1 atm are arbitrarily chosen as zero points. Each encircled group of points represents the response to a given perturbation indicated by the T and p values: T_1 = 10 C, T_2 = 40 C, and $p_1 = 10^6$ Torr. Filled points result from temperature perturbations; open points represent a pressure change. Because none of the three temperature responses (smooth curves) intersects the pressure change points, these two perturbations cannot be mistaken for one another. On this plot, mass changes cause purely horizontal excursions at all three frequencies.

It should be pointed out that the temperature effects in particular and the pressure effects to a lesser extent are not a result of the properties of the ST-quartz device alone, but also a consequence of the manner in which the device is fastened to the PC board. Different thermal expansion coefficients for quartz, the adhesive, and the PC board mean that changing any of the packaging details will alter the shape of the curves of Figure 6. Nevertheless, temperature changes are readily distinguishable from pressure changes or, more importantly, mass changes: variations in surface mass cause very little change in attenuation, and the relationship between velocity shifts at various frequencies is well documented by data like those of Figure 5.

CONCLUSIONS

SAW and APM devices have demonstrated their potential as sensitive detectors of changes in surface mass and other properties in a number of laboratories. While their exquisite mass sensitivity alone will undoubtedly result in a number of specialized applications, the ability to distinguish changes in mass from variations in temperature, pressure, conductivity, permittivity, and viscoelastic properties holds the potential for much more general chemical and physical sensors. Simultaneously measuring the orthogonal acoustic wave propagation factors, velocity and attenuation, at a number of frequencies endows a single MUFAW device with the characteristics of a multisensor using several device technologies.

We gratefully acknowledge the excellent technical assistance of B. J. Lammie of Sandia National Laboratories. This work was supported by the US DOE under contract DE-AC04-76DP00789.

REFERENCES

1. S. J. Martin and A. J. Ricco, "Monitoring Photopolymerization of Thin Films Using SH Acoustic Plate Mode Sensors," *Sensors & Actuators, A (22)*, 712-18 (1990).
2. S. J. Martin and A. J. Ricco, "Effective Utilization of Acoustic Wave Sensor Responses: Simultaneous Measurement of Velocity and Attenuation," *Proc. 1989 IEEE Ultrasonics Symp.*, 1989, pp. 621-25.
3. A. J. Ricco, S. J. Martin, and T. E. Zipperian, "Surface Acoustic Wave Gas Sensor Based on Film Conductivity Changes", *Sensors and Actuators, 8*, 319-333 (1985).
4. T. M. Niemczyk, S. J. Martin, G. C. Frye, and A. J. Ricco, "Acoustoelectric Interaction of Plate Modes with Solutions", *J. Appl. Phys., 64*, 5002-8 (1988).
5. Liquid Phase Sensors Based on Acoustic Plate Mode Devices, A. J. Ricco, S. J. Martin, T. M. Niemczyk, and G. C. Frye, in *Chemical Sensors and Microinstrumentation*, ACS Symposium Series No. 403. Washington, DC: American Chemical Society, 1989, ch. 13.
6. S. J. Martin, A. J. Ricco, T. M. Niemczyk, and G. C. Frye, "Characterization of SH Acoustic Plate Mode Liquid Sensors," *Sensors & Actuators, 20*, 253-68 (1990).
7. A. J. Ricco and S. J. Martin, "Acoustic Wave Viscosity Sensor", *Appl. Phys. Lett., 50*, 1474-76, 1987.
8. D. P. Morgan, *Surface Wave Devices for Signal Processing*. New York: Elsevier, 1985, § 6.2.
9. B. A. Auld, *Acoustic Fields and Waves in Solids*. New York: Wiley, 1973.
10. R. M. White, P. J. Wicher, S. W. Wenzel, and E. T. Zellers, "Plate-Mode Ultrasonic Oscillator Sensors", *IEEE Trans. on Ultrasonics, Ferroelectrics, and Freq. Contr., UFFC-34*, 162-171 (1987).